Supporting Information

Transistor Characteristics of Charge-Transfer Complexes Observed Across a Neutral-Ionic Transition

Tomoki Uekusa,[†] Ryonosuke Sato,[†] Dongho Yoo,[†,‡] Tadashi Kawamoto,[†] and Takehiko Mori[*,†]

Department of Materials Science and Engineering, Tokyo Institute of Technology, O-okayama, Meguro-ku, Tokyo 152-8552, Japan

[*] mori.t.ae@m.titech.ac.jp

Characteristics of non-off transistors

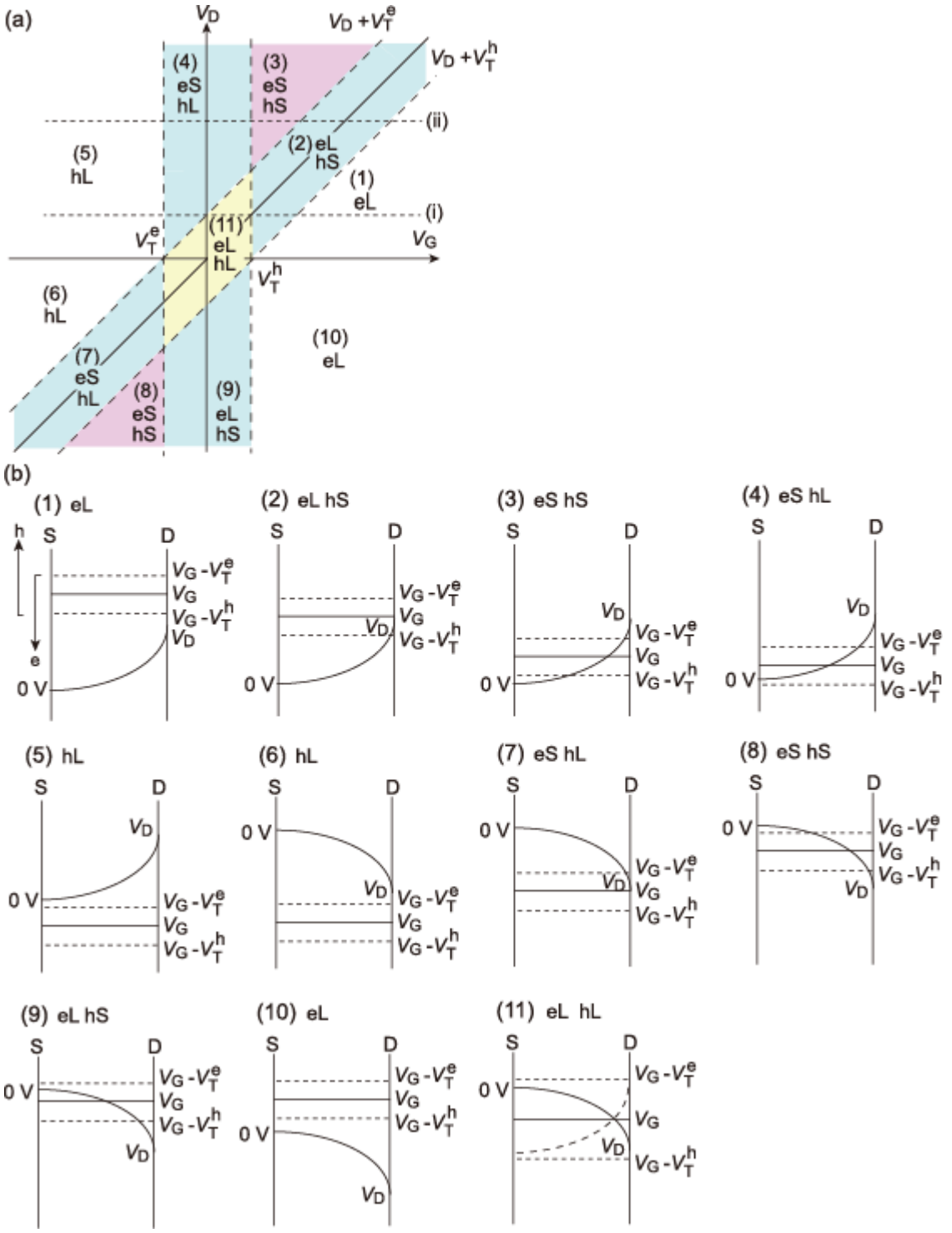

Figure S1. (a) Operation regions of ambipolar transistors with $V_T^e < V_T^h$, and (b) the potential distribution in each region.

The potential distributions in Regions (1) - (11) are represented in Figure S1b, and according to the ordinary gradual channel approximation, the characteristics are represented as shown in Table S1. These formulas are considerably different from those of ordinary ambipolar transistors.[47] When we use the same formula for the linear regions ((1) = (10), (5) = (6), and (11)), $I_D < 0$ for the lower half in Figure S1a. Signs of other characteristics in Table S1 are chosen so as to follow this rule.

Table S1. Characteristics of Non-off Ambipolar Transistors.

Region[a]		Characteristics	Border[b]
(1) (10)	eL	$I_D = \frac{W\mu_e C}{L}[(V_G - V_T^e)V_D - \frac{1}{2}V_D^2]$	$V_G - V_T^h = V_D > 0$
(2)	eL hS	$I_D = \frac{W\mu_e C}{L}[(V_G - V_T^e)V_D - \frac{1}{2}V_D^2] + \frac{W\mu_h C}{2L}(V_G - V_T^h - V_D)^2$	$V_G - V_T^e = V_D > 0$
(3)	eS hS	$I_D = \frac{W\mu_e C}{2L}(V_G - V_T^e)^2 + \frac{W\mu_h C}{2L}(V_G - V_T^h - V_D)^2$	$V_G - V_T^h = 0$
(4)	eS hL	$I_D = \frac{W\mu_e C}{2L}(V_G - V_T^e)^2 - \frac{W\mu_h C}{L}[(V_G - V_T^h)\ V_D - \frac{1}{2}V_D^2]$	$V_G - V_T^e = 0$
(5) (6)	hL	$I_D = -\frac{W\mu_h C}{L}[(V_G - V_T^h)\ V_D - \frac{1}{2}V_D^2]$	$V_G - V_T^e = V_D < 0$
(7)	eS hL	$I_D = -\frac{W\mu_e C}{2L}(V_G - V_T^e - V_D)^2 - \frac{W\mu_h C}{2L}[(V_G - V_T^h)V_D - \frac{1}{2}V_D^2]$	$V_D = V_G - V_T^e < 0$
(8)	eS hS	$I_D = -\frac{W\mu_e C}{2L}(V_G - V_T^e - V_D)^2 - \frac{W\mu_h C}{2L}(V_G - V_T^h)^2$	$V_G - V_T^e = 0$
(9)	eL hS	$I_D = \frac{W\mu_e C}{L}[(V_G - V_T^e)V_D - \frac{1}{2}V_D^2] - \frac{W\mu_h C}{2L}(V_G - V_T^h)^2$	$V_G - V_T^h = 0$
(11)	eL hL	$I_D = \frac{W\mu_e C}{L}[(V_G - V_T^e)V_D - \frac{1}{2}V_D^2] - \frac{W\mu_h C}{L}[(V_G - V_T^h)V_D - \frac{1}{2}V_D^2]$	$V_G - V_T^e > 0$ $V_D > V_G - V_T^h$ $V_G - V_T^h < 0$ $V_G - V_T^e > V_D$

[a] The numbers come from Figure S1. For example, eL hS means linear for electron and saturated for hole.

[b] Border to the following region. (11) is surrounded by these borders.

In the ordinary ambipolar transistors ($V_T^e >> V_T^h$),[45-47] transfer characteristics are not far from those of the independent monopolar transistors (Figure S2a). Simultaneous injection of two carriers occurs only in Regions (3) and (8) (eS hS) with large $V_D > V_T^e - V_T^h$. In the following, we describe only the analysis of the $V_D > 0$ region. The ordinary electron transport occurs in the right side of Figure S2a. The intercept of the conventional square root I_D plot affords V_T^e irrespective of the applied V_D values, where the saturated region continues from V_T^e to $V_T^e + V_D$. The left reversed region ($V_G < 0$) is of no use for estimating V_T^h, though the slope affords μ_h.

When V_T^e is small (Figure S2c), the square root I_D plot is not entirely straight because the linear region appears above a comparatively small $V_G > V_T^e + V_D$. Even in this case, extrapolation of the square root I_D plot in the small $V_G < V_T^e + V_D$ saturated region affords V_T^e. Extrapolation of the linear region ($V_G > V_T^e + V_D$) affords $V_T^e + (1/2)V_D$, as evident from the equation of the linear Region (1). When $(1/2)V_D$ is subtracted from the intercept, we can obtain V_T^e. However, this method is not very reliable. The output characteristics (Figure S2d) shows a clear flat region, and V_G affording the smallest flat region gives V_T^e. In Figure S2d, the flat regions of the $V_G = 0$ and 20 V curves are close to the horizontal line ($I_D = 0$), and this is in agreement with $V_T^e = 10$ V. In general, the existence of the flat region in the output characteristics is reliable evidence of the presence of the off region ($V_T^e > V_T^h$).

However small is applied V_D, the transfer characteristics of a non-off transistor do not drop to $I_D = 0$ (Figure S2e). The square root I_D plot is not straight, and the extrapolation is largely different from V_T^e. It is noteworthy that the output characteristics no more have a flat region (Figure S2f).

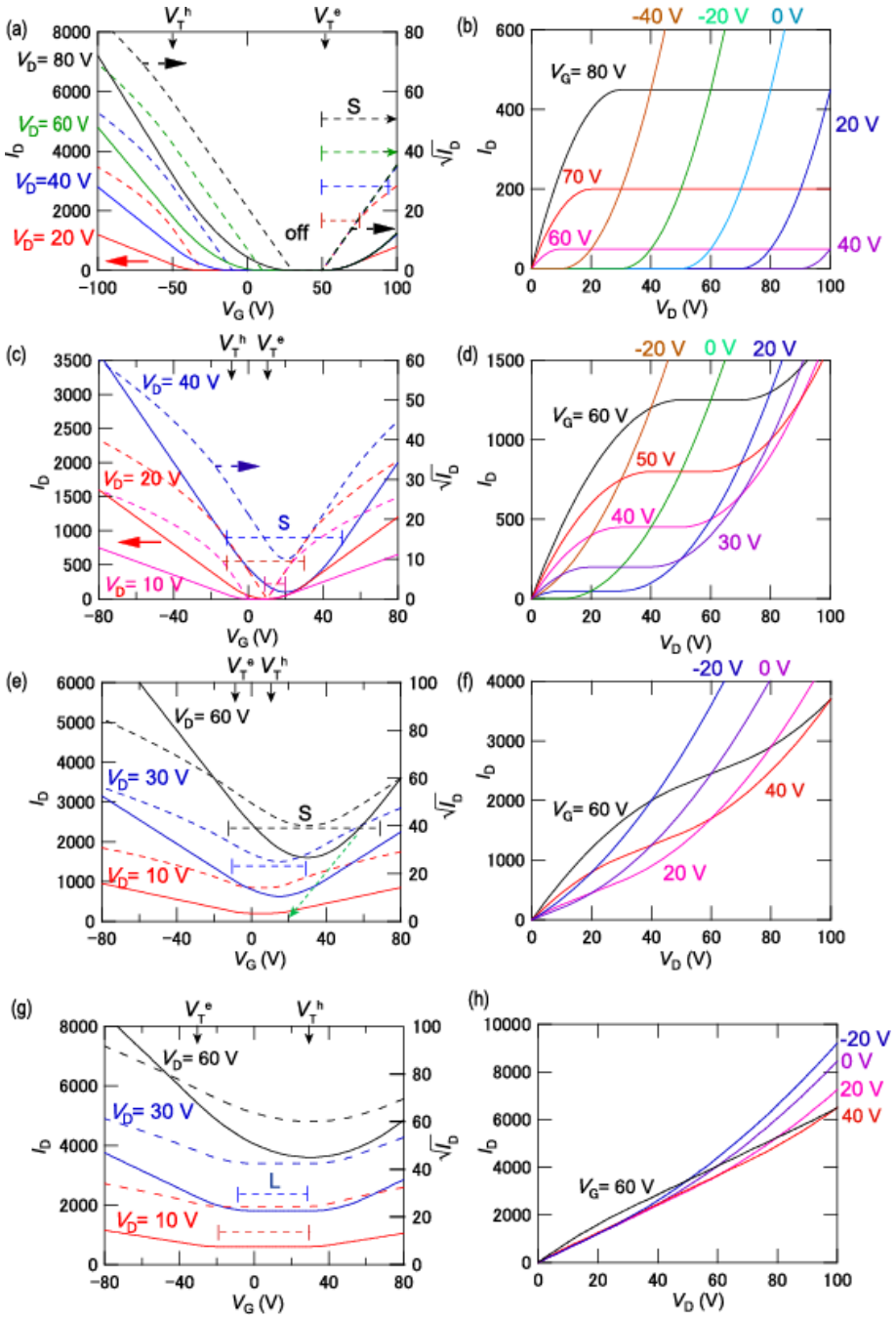

Figure S2. (a) Calculated transfer characteristics of an ordinary transistor with a large off region (V_T^e = 50 V, V_T^h = −50 V, and μ_e = μ_h). Solid curves are linear I_D plots and dashed curves are square root I_D plots. S means the saturated region. (b) The corresponding output characteristics. (c) Transfer characteristics with a small off region (V_T^e = 10 V and V_T^h = −10 V). (d) The corresponding output characteristics. (e) Transfer characteristics of a non-off transistor (V_T^e = −10 V and V_T^h = 10 V). Note that V_T^e and V_T^h are inverted compared to (c). (f) The corresponding output characteristics. (g) Transfer characteristics with a large non-off region (V_T^e = −30 V and V_T^h = 30 V). L means the linear Region (11). (h) The corresponding output characteristics.

Redox potentials

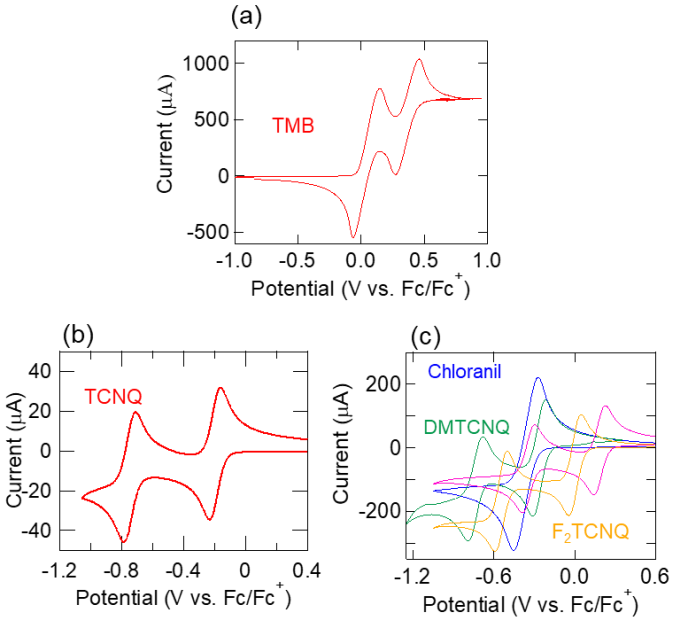

Figure S3. Cyclic voltammetry of (a) TMB, (b) TCNQ and (c) chloranil, DMTCNQ, TCNQ, F_2TCNQ, and F_4TCNQ.

Table S2. Redox potentials (*vs.* ferrocene/ferrocenium).

Complex	$E_{1/2}{}^1$ (V)	$E_{1/2}{}^2$ (V)
TMB	0.04	0.48
Chloranil	−0.36	–
DMTCNQ	−0.26	−0.65
TCNQ	−0.20	−0.74
F_2TCNQ	0.00	−0.55
F_4TCNQ	0.19	−0.30

Crystal structures

TMB crystals are not strictly isostructural depending on the packing patterns of the columns along the layer axis (//*a* in Figure 3a) and along the adjacent columns (//*b* in Figure 3a); the differences are summarized in Table S3. In the chloranil and bromanil complexes (space group *C*2/*m*), all molecules in the adjacent columns and layers are parallel to each other (Figure S4a). Similarly to the DMTCNQ complex (Figure S4c), the long axes of the adjacent layers in the TCNQ and F_2TCNQ complexes are alternately tilted (Figures S4e and g). In the latter two crystals ($P2_1/n$), however, the molecular plane levels in the adjacent columns are slightly deviated (Figures S4f and h). In the F_4TCNQ complex (*C*2/*m*), all molecular long axes are parallel again (Figure S4i), but the level shift remains (Figure S4j). These small differences come from the packing pattern of the columns, but the structure of a single column is essentially the same.

Table S3. Summary of the TMB crystals.

Complex	Space group	Long axes along the layers (//*a*)[a]	Level shift on the side (//*b*)[a]
Chloranil	*C*2/*m*	Parallel	N
Bromanil	*C*2/*m*	Parallel	N
DMTCNQ	*Pnnm*	Tilted	N
TCNQ	$P2_1/n$	Tilted	Y
F_2TCNQ	$P2_1/n$	Tilted	Y
F_4TCNQ	*C*2/*m*	Parallel	Y

[a] Axes of the DMTCNQ complex.

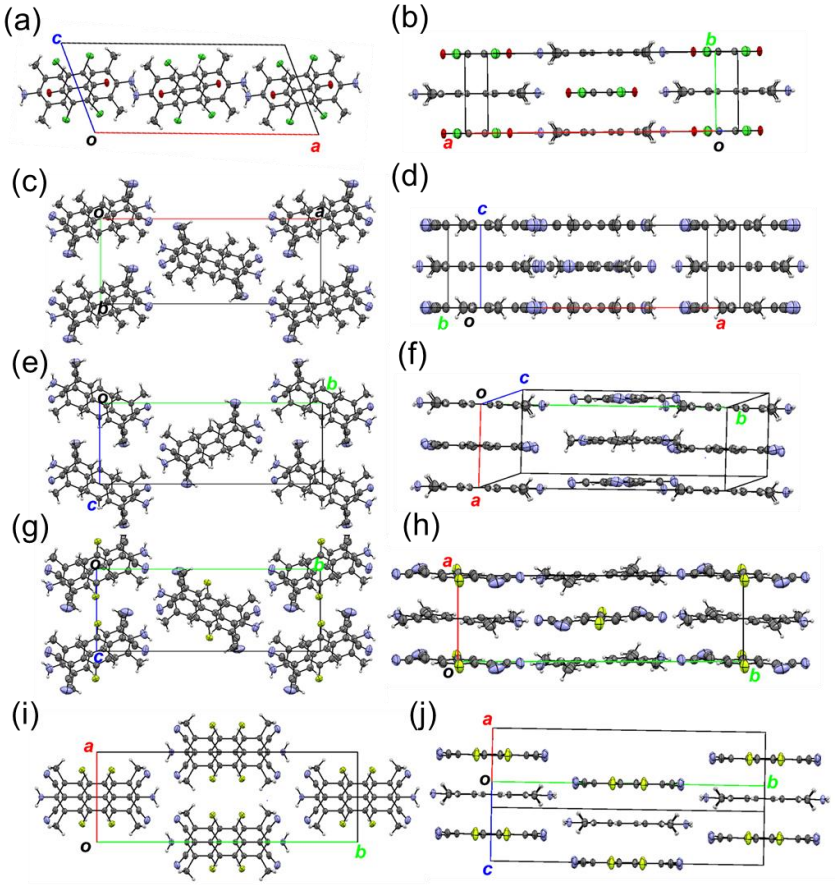

Figure S4. Crystal structures of (a)(b) (TMB)(chloranil), (c)(d) (TMB)(DMTCNQ), (e)(f) (TMB)(TCNQ), (g)(h) (TMB)(F_2TCNQ), and (i)(j) (TMB)(F_4TCNQ), respectively viewed along the stacking axes, and viewed along the molecular long axes.[24,25]

Degree of charge transfer

Charge-transfer degree ρ_{BL} of the TCNQ complexes was estimated from the bond lengths of TCNQ (Table S4).[S1]

$$\rho_{BL} = 27.94 \times [(a + c) / (b + d)] - 26.28$$

ρ of the F_4TCNQ complex was estimated from a different equation.[S2]

$$\rho_{BL} = -45.756 \times [c / (b + d)] + 21.846$$

Charge-transfer degree ρ_{IR} was estimated from the C≡N stretching mode $\nu_{C\equiv N}$ of the IR spectra (Figure S5) using

$$\nu_{C\equiv N} = 2227 - 44\rho_{IR} \quad (cm^{-1})$$

as listed in Table S4.[S3]

Table S4. Bond lengths, the C≡N stretching mode, and the resulting ρ of the CT complexes.[a]

	DMTCNQ	TCNQ	F_2TCNQ	F_4TCNQ
a (Å)	1.350	1.354	1.355	1.350
b (Å)	1.427	1.437	1.434	1.435
c (Å)	1.392	1.389	1.378	1.377
d (Å)	1.425	1.426	1.4395	1.434
ρ_{BL}	0.48	0.49	0.67	0.83
$\nu_{C\equiv N}$ (cm^{-1})	2211	2203		
ρ_{IR}	0.36	0.54		

[a] *b* and *d* are averaged.

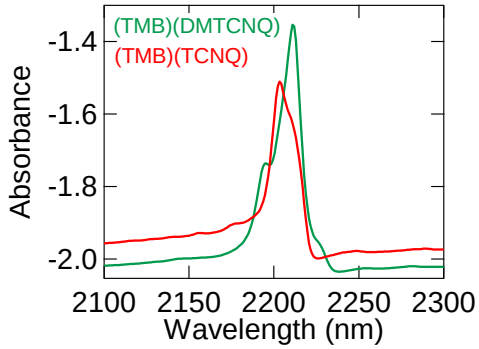

Figure S5. C≡N stretching mode of the IR spectra of (TMB)(DMTCNQ) and (TMB)(TCNQ).

Single-crystal transistors

Single-crystal transistors of (TMB)(chloranil), (TMB)(DMTCNQ), and (TMB)(TCNQ) were prepared by depositing the chlorobenzene solutions (Figure S6a-c). Transistors of (TMB)(F_2TCNQ), (TMB)(F_4TCNQ), and (TMB)(bromanil) were made by pasting the crystals (Figure S6d-f), but the bromanil transistors did not show transistor properties. Thickness of the films was measured by using a Kosaka Surfcorder ET200.

Table S5. Dimensions of single-crystal transistors shown in Figures 3 and 4.

Complex	Fabrication	L (μm)	W (μm)	d (μm)
Chloranil	Drop cast	75	13	2.0
DMTCNQ	Drop cast	13	3.2	2.0
TCNQ	Drop cast	75	25	2.5
F_2TCNQ	Paste	37	13	25
F_4TCNQ	Paste	30	10	20

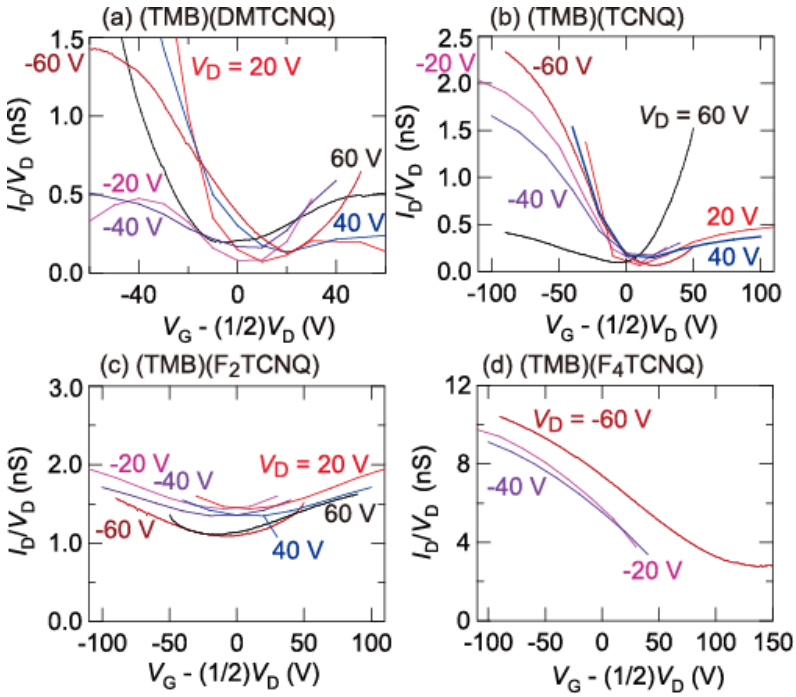

Figure S6. Normalized transfer characteristics of thin-film transistors of (a) (TMB)(DMTCNQ), (b) (TMB)(TCNQ), (c) (TMB)(F_2TCNQ), and (d) (TMB) (F_4TCNQ).

Calculation of effective transfer integrals

Molecular orbital calculations in the B3LYP* level with TZP basis set were performed using the the Amsterdam Density Functional (ADF) program.[S4] Energy differences in Eq. S1 were taken from the triad calculations. These molecular orbitals were very similar to the results of the AM1 calculations.[S5] In order to estimate t_{DA}, the frozen orbital approximation was adopted, where the molecular orbitals were extracted and used to calculate the intermolecular transfer integrals.[S6]

Transport in DA crystals have been discussed in analogy with DA polymers on the basis of superexchange transfer.[8,S7-S11] There are large transfers t_{DA} between the TMB HOMO and the acceptor LUMO in the present TMB complexes (Table S6), so that the effective electron and hole transfers t^{eff} in mixed stacks are given by the HOMO-LUMO only partition theory.[8,S10]

$$t^{eff} = \frac{t_{DA}^2}{E_A - E_D} \qquad \text{Eq. S1}$$

Since $E_A - E_D$ decreases with increasing the acceptor ability, t^{eff} increases (Table S7). This is reproduced by the triad calculation as well. This accounts for the observed increase of the mobility (Figure S7). The observed mobility of the F_2TCNQ complex is anomalously small in comparison with the other complexes. Note that $E_A - E_D$ does not diverge even at $E_A = E_D$ because $E_A - E_D$ of a complex is larger than the energy difference of the independent molecules due to t_{DA}. This is a similar situation to Eq. 8. Accordingly, the increase of t^{eff} (and μ) toward the ionic limit is comparatively mild.

Table S6. Effective transfer integrals (meV).

Complex	Partition			Triad	
	$E_A - E_D$	t_{DA}	t^{eff}	t_e^{eff}	t_h^{eff}
Chloranil	1345	323	78	162	111
DMTCNQ	1158	350	106	164	140
TCNQ	1104	370	124	161	136
F_2TCNQ	997	478	229	181	158
F_4TCNQ	896	371	154	199	216

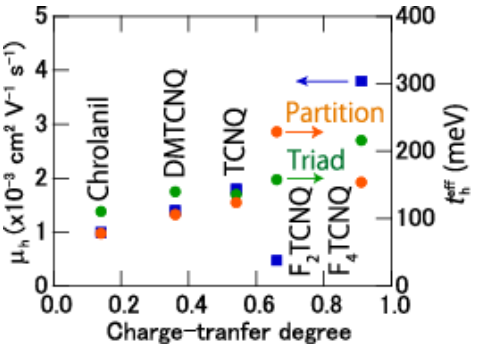

Figure S7. Observed mobility and calculated t_h^{eff}.

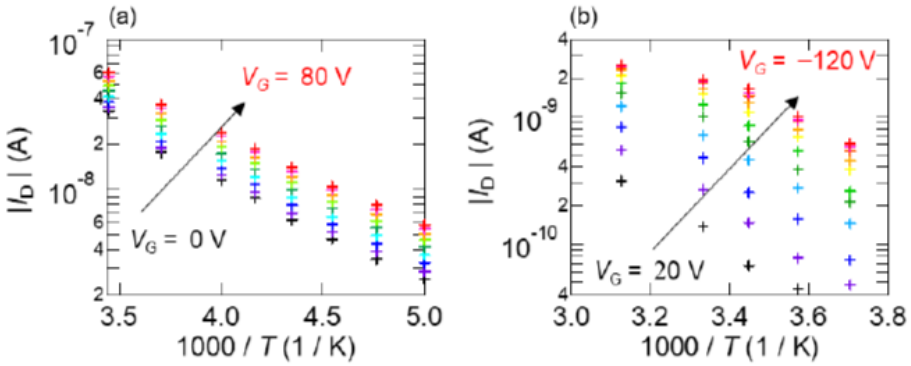

Figure S8. Arrhenius plots of I_D in (a) (TMB)(TCNQ), and (b) (TMB)(chloranil).

Energy band of a mixed-stack chain

Energy band of a mixed-stack chain (Figure S9) having a transfer integral t_{DA} between the donor HOMO (with the energy E_D) and the acceptor LUMO (with the energy E_A) is calculated from

$$\begin{vmatrix} E_A - E & t_{DA} \\ t_{DA} & E_D - E \end{vmatrix} = 0$$

.

The solution is as follows.

$$E = \frac{E_A + E_D}{2} \pm \sqrt{\left(\frac{E_A - E_D}{2}\right)^2 + 4t_{DA}{}^2 \cos^2 ka}$$

Since the inside of the square root is never smaller than the first term, this energy band is represented by Figure 9b, where the band gap is given by $E_A - E_D$.

Historically, derivations of Eqs. 6-9 have been discussed in Refs. S11-S13 in addition to Refs. 21 and 69.

Figure S9. Energy levels of a mixed-stack chain.

References

(S1) Umland, T. C.; Allie, S.; Kuhlmann, T.; Coppens, P. Relation between Geometry and Charge Transfer in Low-Dimensional Organic Salts. *J. Phys. Chem.* **1988**, *92*, 6456–6460.

(S2) Sutton, A. L.; Abrahams, B. F.; D'Alessandro, D. M.; Elliott, R. W.; Hudson, T. A.; Robson, R.; Usov, P. M. Structural and Optical Investigations of Charge Transfer Complexes Involving the F_4TCNQ Dianion. *CrystEngComm* **2014**, *16*, 5234-5243.

(S3) Chappell, J. S.; Bloch, A. N.; Bryden, W. A.; Maxfield, M.; Poehler, T. O.; Cowan, D. O. Degree of Charge Transfer in Organic Conductors by Infrared Absorption Spectroscopy. *J. Am. Chem. Soc.* **1981**, *103*, 2442–2443.

(S4) ADF2017.109; Scientific Computing & Modeling (SCM). Theoretical Chemistry; Vrije Universiteit: Amsterdam, The Netherlands. http://www.scm.com.

(S5) Dewar, M. J. S. E.; Zoebisch, G.; Healy, E. F.; Stewart, J. J. P. Development and Use of Quantum Mechanical Molecular Models. 76. AM1: a New General Purpose Quantum Mechanical Molecular Model, *J. Am. Chem. Soc*. **1985**, *107*, 3902-3909.

(S6) Mori, T.; Kobayashi, A.; Sasaki, Y.; Kobayashi, H.; Saito, G.; Inokuchi, H. The Intermolecular Interaction of Tetrathiafulvalene and Bis(ethylenedithio) tetrathiafulvalene in Organic Metals. Calculation of Orbital Overlaps and Models of Energy-Band Structures, *Bull. Chem. Soc. Jpn.,* **1984**, *57*, 627-633.

(S7) Cheng, C.; Geng, H.; Yi, Y.; Shuai, Z. Super-Exchange-Induced High Performance Charge Transport in Donor-Acceptor Copolymers, *J. Mater. Chem. C* **2017**, *5*, 3247-3253.

(S8) Zhu, L.; Yi, Y.; Li, Y.; Kim, E.; Coropceanu, V.; Bredas, V. J. Prediction of Remarkable Ambipolar Charge-Transport Characteristics in Organic Mixed-Stack Charge-Transfer Crystals, *J. Am. Chem. Soc*. **2012**, *134*, 2340-2347.

(S9) Zhu, L.; Yi, Y.; Fonari, A.; Corbin, N. S.; Coropceanu, V.; Bredas, J. Electronic Properties of Mixed-Stack Organic Charge-Transfer Crystals, *J. Phys. Chem. C* **2014**, *118*, 14150-14156.

(S10) Geng, H.; Zheng, X.; Shuai, Z.; Zhu, L.; Yi, Y. Understanding the Charge Transport and Polarities in Organic Donor–Acceptor Mixed-Stack Crystals: Molecular Insights from the Super-Exchange Couplings, *Adv. Mater*. **2015**, *27*, 1443-1449.

(S11) McConnell, H. M.; Hoffman, B. M.; Metzger, R. M. Charge Transfer in Molecular Crystals, *Proc. Nat. Acad. Sci. U. S. A.* **1965**, *53*, 46-50.
(S12) Strebel, P. J.; Soos, Z. G. Theory of Charge Transfer in Aromatic Donor-Acceptor Crystals, *J. Chem. Phys*. **1970**, *53*, 4077-4090.
(S13) Saito, G.; Yoshida, Y. Development of Conductive Organic Molecular Assemblies: Organic Metals, Superconductors, and Exotic Functional Materials, *Bull. Chem. Soc. Jpn*. **2007**, *80*, 1-137.